International Journal of Heat and Mass Transfer 150 (2020) 119273

Contents lists available at ScienceDirect

International Journal of Heat and Mass Transfer

journal homepage: www.elsevier.com/locate/hmt

Mixed dropwise-filmwise condensation heat transfer on biphilic surface

Jian Xie[a,b], Qingting She[a], Jinliang Xu[a,b,*], Cong Liang[a], Wenxiao Li[a]

[a] Beijing Key Laboratory of Multiphase Flow and Heat Transfer for Low Grade Energy Utilization, North China Electric Power University, Beijing 102206, China

[b] Key Laboratory of Power Station Energy Transfer Conversion and System (North China Electric Power University), Ministry of Education, China

ARTICLE INFO

Article history:
Received 23 September 2019
Revised 27 November 2019
Accepted 23 December 2019

Keywords:
Condensation
Heat transfer enhancement
Biphilic surface
Droplet detachment
Wettability

ABSTRACT

Condensation heat transfer on biphilic surface is investigated. The surface periodically populates hydrophobic stripes each having a coating layer thickness δ_p and a width W_{DWC}, and hydrophilic stripes each having a width W_{FWC}. The proposed model includes dropwise condensation on hydrophobic stripe, filmwise condensation on hydrophilic stripe, and droplet detachment radius r_{max} criterion for heat-mass coupling between the two wettabilities regions. The r_{max} is the minimum of detachment radii determined by droplet removal modes of double-sides-suction DSS, one-side-suction OSS and sliding, where DSS is a special case of OSS for droplet located at hydrophobic stripe centerline. Simulation results matched the measured heat transfer data well. Optimal width of hydrophobic stripe W^o_{DWC} is found to be dominated by δ_p and W_{FWC}, but other parameters weakly influence W^o_{DWC}. Interfaced by a $\delta_p - W_{FWC}$ transition curve, a heat transfer regime map is presented to contain Regime I for possible heat transfer enhancement and Regime II for heat transfer deterioration. Regime I enhances heat transfer if W_{DWC} approaches W^o_{DWC}, but may deteriorate heat transfer if W_{DWC} deviates W^o_{DWC} too much. The maximum heat transfer enhancement ratio is 1.67 compared with purely hydrophobic surface. Regime II always deteriorates heat transfer. Our work provides a general guideline to design biphilic surface for performance improvement.

1. Introduction

Condensation heat transfer enhancement is important to reduce equipment size, metallic consumption and investment cost of condensers. Condensation includes filmwise condensation (FWC) on hydrophilic surface and dropwise condensation (DWC) on hydrophobic surface. The liquid film thickness plays important role on FWC [1]. Various methods have been proposed to decrease liquid film thickness to enhance FWC [2–4]. Heat transfer coefficient of DWC is one or two magnitudes higher than that of FWC [5]. For DWC, the droplet detachment radius r_{max} greatly affects heat transfer [6], noting that r_{max} is also the maximum radius of droplet that can stay on hydrophobic surface. When a droplet reaches r_{max}, the droplet can be detached. DWC can be enhanced by reducing r_{max}. The value of r_{max} depends on droplet detachment modes. Xie et al. [7,8] investigated droplet detachment modes on uniform wettability surfaces, including sliding, rolling and jumping. For contact angle $\theta < 126^o$, droplet detaches the surface by sliding mode. For $\theta > 147^o$, droplet detaches the surface by rolling mode. Besides, the droplets-coalescence-induced-jumping can occur on nanostructured superhydrophobic surface, decreasing r_{max} [9]. Such surface is expected to enhance DWC.

Many studies have been reported about DWC on superhydrophobic surface. Wen et al. [10] demonstrated a stable jumping droplet condensation on three-dimensional superhydrophobic nanowire networks, showing that over a wide range of subcooling, the dissipated heat flux can be two times of that on hydrophobic surface without nanostructure. Various challenges exist for DWC on superhydrophobic surface [5]: (1) The nanostructured surface behaves both positive and negative effects on DWC. The decreased r_{max} and increased number of drop-nucleation-sites enhance DWC, but the surface introduces an additional thermal resistance to deteriorate DWC [9]. (2) DWC can be deteriorated due to flooding at high saturation vapor pressure or high surface subcooling [11–14]. (3) After long-term operation, the nanostructured surface may be destroyed. The droplet detachment modes change from jumping to rolling or sliding, and heat transfer is strongly deteriorated [7,15]. Thus, it is necessary to seek other solutions to enhance DWC.

Murphy and Boreyko [16] performed DWC experiment on a hydrophobic surface, whose droplets are sucked by an opposite hydrophilic surface. They observed the decreased droplet detachment

* Corresponding author at: Beijing Key Laboratory of Multiphase Flow and Heat Transfer for Low Grade Energy Utilization, North China Electric Power University, Beijing 102206, China.
E-mail address: xjl@ncepu.edu.cn (J. Xu).

https://doi.org/10.1016/j.ijheatmasstransfer.2019.119273
0017-9310/

Nomenclature

A	area, m^2
A_1	parameter in Eq. (25), m
A_2	parameter in Eq. (12), mK/W
A_3	parameter in Eq. (12), m^2K/W
a	area ratio of hydrophobic stripe to hydrophilic stripe, $a = W_{DWC}/W_{FWC}$
B	parameter in Eq. (25), m
B_1	parameter in Eq. (12)
B_2	parameter in Eq. (12)
Bi	Biot number
C	parameter in Eq. (25), m
e_A	mean absolute deviation
e_R	average deviation
f_{DWC}	ratio of hydrophobic stripes area to the total biphilic surface area
g	gravitational acceleration, m/s^2
h	heat transfer coefficient, $W/(m^2K)$
h_i	heat transfer coefficient at vapor-liquid interface, $W/(m^2K)$
h_{lv}	latent heat of evaporation, kJ/kg
i	index of grid from the margin
$N(r)$	population density of large droplets, m^{-2}
N_c	droplet nucleation site density, m^{-2}
n	grid number in the width of $W_{DWC}/2$
$\bar{n}$	number of hydrophobic (or hydrophilic) stripes
$n(r)$	population density of small droplets, m^{-2}
$Q(r)$	heat transfer rate of a single drop with size of r, W
P_{sat}	saturation vapor pressure, Pa
q_{DWC}	local heat flux on hydrophobic stripe, W/m^2
$q_{BI,\ DWC}$	average heat flux on hydrophobic stripe, W/m^2
$q^*_{BI,DWC}$	effective heat flux of liquid transferred from hydrophobic stripe to hydrophilic stripe, W/m^2
R	radius of the biphilic surface, m
r	droplet radius, m
r_c	half of average spacing between neighboring nucleation sites, m
r_{max}	droplet detachment radius, m
$r_{max,1}$	r_{max} calculated by Eq. (3), m
$r_{max,2}$	r_{max} calculated by Eq. (4), m
$r_{max,3}$	r_{max} calculated by Eq. (6), m
r_{min}	minimum droplet nucleation radius, m
r_{slide}	droplet detachment radius for sliding mode, m
T_{sat}	saturation vapor temperature, °C
T_w	surface temperature, °C
t_c	liquid suction time, s
$\bar{u}$	mean liquid film velocity on hydrophilic stripe, m/s
V	total volume flow rate of condensate, m^3/s
V_{FWC}	volume flow rate of self-condensation on hydrophilic stripes, m^3/s
V_{trans}	volume flow rate of condensate transferred from hydrophobic stripes, m^3/s
W	width, m
$W_{DWC,\ c}$	critical width of hydrophobic stripe for onset of sliding, m
W^o_{DWC}	optimal width of hydrophobic stripe, m
x	distance from the margin to the droplet center-mass location, m

Greek symbols

Δ	deviation of droplet center-mass location from the hydrophobic stripe centerline, m
ΔT	wall subcooling, °C
Δx	grid size of distance from the margin to the droplet center-mass location, m
δ	thickness, m
λ	thermal conductivity, W/(m K)
μ	viscosity of condensate, Pa•s
θ	equilibrium contact angle on hydrophobic stripe, °
θ_a	advancing contact angle on hydrophobic stripe, °
θ_r	receding contact angle on hydrophobic stripe, °
ρ	density, kg/m^3
σ	surface tension, N/m
σ_n	standard deviation
Ω	contact angle hysteresis, $\Omega = \cos\theta_r - \cos\theta_a$

Subscript

BI	biphilic stripe surface
c	copper
DWC	dropwise condensation on hydrophobic stripe
exp	experiment data
FWC	filmwise condensation on hydrophilic stripe
HB	purely hydrophobic surface
HL	purely hydrophilic surface
l	liquid
max	maximum value
p	polymer
pre	prediction value
v	vapor

size. Ji et al. [17] successfully demonstrated a vapor-chamber heat pipe, by using a superhydrophobic surface for condensation and a superhydrophilic surface for evaporation. It is shown that both evaporation and condensation are enhanced in the phase change system. The performance improvement is attributed to the liquid mass transport from superhydrophobic surface to superhydrophilic surface. The above system can be referred to the Janus system. The opposite wettability surfaces are spatially arranged at different planes. On the other hand, biphilic surface contains both hydrophobic region and hydrophilic region on a same plane, which may be the next generation of functional surface for condensation improvement.

The mixed dropwise-filmwise condensation studies on biphilic stripe surface are summarized in Table 1. The early studies can be tracked back to 1980s [18–20]. Due to the limit of fabrication techniques, both hydrophilic and hydrophobic stripes had the widths in ~mm scale. These studies showed that condensation heat transfer coefficient on biphilic stripe surface (h_{BI}) is lower than that on purely hydrophobic surface (h_{HB}), but larger than the mean value using the heat transfer coefficient on either purely hydrophilic or hydrophobic surfaces weighted by the areas ratio of the two wettability regions. Subsequently, the stripe widths for both regions are narrowed for heat transfer improvement [21,22]. Recently, with the fast development of micro-fabrication techniques, the stripe width is further decreased to sub-millimeter. Garimella et al. [23] observed the decreased droplets size. Mahapatra et al. [24] and Wu et al. [25] demonstrated that the biphilic stripe surfaces raised condensate collection efficiencies under wet air condition. Alwazzan et al. [26] showed an 80% of heat transfer improvement compared to purely hydrophobic surface. Peng et al. [27] noted that the geometry parameters obviously influence heat transfer. The value of h_{BI} increases with decrease of hydrophilic stripe width, and there is an optimal width of hydrophobic stripe W^o_{DWC} to reach maximum h_{BI} [28]. However, theoretical analysis of W^o_{DWC} is seldom reported in the literature.

The objective of this paper is to present a comprehensive condensation heat transfer model on biphilic stripe surface, and explore the conditions and mechanisms for heat transfer en-

Table 1
Representative investigations of condensation on biphilic stripe surface.

Reference	substrate	hydrophilic material	hydrophobic material	W_{FWC}(mm)	W_{DWC}(mm)	θ (°)	working fluid	comments
Kumagai et al. [18]	Cu plate	Cu	PTFE	3–7	0.5–7	–	steam	➢ $h_{HL}<h_{BI}<h_{HB}$ ➢ h is larger than the weighted mean of h_{HL} and h_{HB}.
Derby et al. [21]	Cu plate	Cu	PTFE	0.43–1.10	–	120	steam	➢ $h_{HL}<h_{BI}<h_{HB}$ ➢ h_{HL} is a strong function of vapor quality and mass flux. However, h_{BI} and h_{HB} are independent on vapor quality and mass flux.
Mahapatra et al. [24]	Al plate	Al_2O_3	Al	0.3–0.4	0.4–2.5	78	humidified air	➢ Hybrid surface inspired by banana leaf improves condensate collection rate. ➢ There exists an optimal W_{FWC}/W_{DWC} to achieve best condensate collection rate.
Alwazzan et al. [26]	Cu tube	Cu	n-octadecyl mercaptan	0.2–0.6	0.2–1.0	90	air-steam mixtures	➢ Maximally, $h_{BI,max}=4.8h_{HL}$; $h_{BI,max}=1.8h_{HB}$. ➢ An optimum W_{FWC} exists to achieve $h_{BI,max}$.
Peng et al. [27]	Cu plate	Cu	n-octadecyl mercaptan	0.45–2.50	0.46–2.30	120	steam	➢ Maximally, $h_{BI,max}=1.23h_{HB}$. ➢ An optimum W_{DWC} exists to achieve $h_{BI,max}$. ➢ h_{BI} decease with the increase of W_{FWC}.
Peng et al. [28]	plate	–	–	0.5–1.0	0.1–1.7	70–120	steam	➢ Condensation heat transfer model is developed based on the assume: $r_{max}=W_{DWC}/2/\sin\theta$. ➢ The optimum W_{DWC} increases with increasing W_{FWC} and ΔT, but decreases with increasing θ.

hancement on such surface. The paper is organized as follows. Section 2 presents the condensation model on biphilic surface. Droplets detachment modes on hydrophobic stripe, and liquid film thickness on hydrophilic stripe are paid great attention. Section 3 regards results and discussion. Section 3.1 compares the present model with available model in the literature, and verifies simulation results by experiments. Section 3.2 analyzes why an optimal width of hydrophobic stripe W^{o}_{DWC} exists to achieve maximum heat transfer, and explores effects of various parameters on W^{o}_{DWC}. Section 3.3 presents a heat transfer regime map including a possible heat transfer enhancement regime and a heat transfer deterioration regime. Conclusions are summarized in Section 4.

2. Numerical simulation

2.1. The problem statement

Condensation on a biphilic surface is investigated. The surface contains periodically arranged hydrophobic stripes and hydrophilic stripes (see Fig. 1). The surface is vertically positioned. DWC occurs on hydrophobic stripes, each having a width of W_{DWC} and a coating layer thickness of δ_p. The static, advancing and receding contact angle are recorded as θ, θ_a and θ_r respectively. FWC occurs on hydrophilic stripes, which can be considered as open channels for liquid drainage. Liquid in open channels comes from self-condensed liquid in the channel and liquid collected from hydrophobic stripes. Before presenting the mathematical model, assumptions are summarized as follows.

Different temperatures on biphilic surface: The biphilic surface has hydrophilic region of exposed copper and hydrophobic region with a coating layer. The two regions have different surface temperatures due to an additional conduction thermal resistance of the coating layer, which is properly treated in this paper. However, the temperature of the copper surface not including the coating layer is assumed to be uniform. The temperature uniformity of the copper surface can be verified by Biot number: $Bi = h_{BI}\delta_c/\lambda_c$, where h_{BI} is the overall condensation heat transfer coefficient, δ_c and λ_c are thickness and thermal conductivity of copper, respectively. Practically, parameters such as $h_{BI} = 10$ kW/m^{2}K, $\delta_c = 1$ mm and $\lambda_c = 380$ W/(mK) yield $Bi = 0.027 < 0.1$, indicating that copper can have uniform temperature [29]. Similar treatment can be found in Refs. [28,30]. Here, the surface subcooling is defined as $\Delta T = T_{sat} - T_w$, where T_{sat} is the saturation temperature of pure water-vapor, T_w is the copper surface temperature, not the coating layer temperature.

Sufficient liquid suction capability by hydrophilic stripe: It is assumed that hydrophilic stripes have sufficient liquid suction capability. This assumption is valid due to two reasons. First, condensation converts vapor to liquid. Liquid density can be 2~3 magnitudes larger than vapor density, indicating a larger liquid collection and transport capability by hydrophilic stripe. Second, it seems that there is a limit for liquid suction by hydrophilic stripe when hydrophobic stripe is extremely wide. However, only the droplets on hydrophobic stripe near the margin are necessary to be sucked by hydrophilic stripe. Droplets on the center area of hydrophobic stripe can be self-detached by sliding due to gravity. In other words, the increase of hydrophobic stripe width increases the liquid to be sucked by hydrophilic stripe, but this increase trend stopes when the droplet self-departure effect begins.

Negligible liquid suction time by hydrophilic stripe: The liquid suction time can be scaled by $t_c = \sqrt{\rho_l r^3/\sigma}$, where ρ_l, r and σ are the liquid density, droplet radius and surface tension, respectively. Practically, t_c is ~10 ms for a water droplet radius equivalent to its capillary length. Ghosh et al [31] observed $t_c = 35$ ms for a droplet with $r = 1.06$ mm during liquid suction. On the contrary, a droplet lifetime including nucleation and growth before departure is ~1 s [6,32]. It is concluded that the liquid suction time is two magnitudes shorter than the droplet lifetime. Besides, the attraction force between liquid molecules is sufficiently large to suppress the contact angle hysteresis induced resistance force on the droplet tail. Thus, it is reasonable to assume that a droplet suddenly disappears on hydrophobic stripe when it contacts the margin between two neighboring stripes.

2.2. Mathematical model

2.2.1. Overall heat transfer on biphilic surface

Overall heat transfer coefficient h_{BI} is defined as the heat transfer coefficients in the two regions weighted by the area ratio of the two regions, which is

$$h_{BI} = f_{DWC}\left(h_{BI,DWC} + \frac{W_{FWC}}{W_{DWC}} h_{BI,FWC}\right) \tag{1}$$

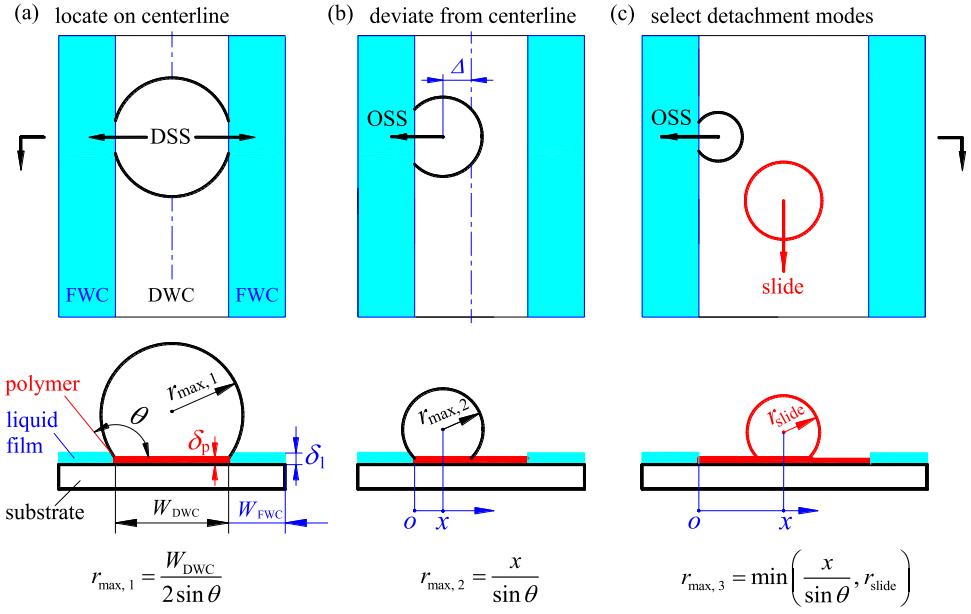

Fig. 1. Droplet detachment modes (a: double-side-suction DSS, b: one-side-suction OSS, c: mixed detachment modes with OSS and sliding).

where $h_{BI,DWC}$ and $h_{BI,FWC}$ are the heat transfer coefficients on hydrophobic stripe and hydrophilic stripe, respectively, f_{DWC} is the ratio of hydrophobic stripes area to the total area:

$$f_{DWC} = \frac{W_{DWC}}{W_{DWC} + W_{FWC}} \tag{2}$$

Thus, the determination of h_{BI} turns to calculate the heat transfer coefficients in the two regions. The droplet detachment radius r_{max} is the coupling parameter to determine the condensation heat transfer on the two regions. When a droplet reaches r_{max}, it disappears on hydrophobic stripe but is transported to the open channel. First, r_{max} appears as the upper limit of integral for DWC on hydrophobic stripe to determine $h_{BI,\,DWC}$, which is regarded as the direct effect. Second, r_{max} determines liquid mass transfer from hydrophobic stripe to influence liquid film thickness and heat transfer on hydrophilic stripe, which is regarded as the indirect effect.

Fig. 1 shows that r_{max} is dependent on x, which is the distance from the margin to the droplet center mass location. As a special case, when a droplet is located at the hydrophobic stripe centerline, the droplet cannot be detached until the droplet footprint size reaches the half width of hydrophobic stripe (see Fig. 1a). Generally, droplets can populate anywhere on hydrophobic stripe. If a droplet deviates from the hydrophobic stripe centerline, r_{max} should be decreased, because it is closer to one margin (see Fig. 1b). Besides, for large W_{DWC}, it is possible for some droplets to slide on hydrophobic stripes, under which the corresponding droplets do not enter the hydrophilic stripe (see Fig. 1c). The model presented by Peng et al. [28] only involves the special case treatment shown in Fig. 1a. The contribution of this paper is to present a comprehensive analysis of all the droplet detachment modes, which are key to determine the coupling heat transfer on biphilic surface. The r_{max} determination and condensation heat transfer in the two regions are consecutively discussed in following sections.

2.2.2. Droplet detachment modes and sizes on hydrophobic stripe

Double-sides-suction (DSS) ensures the contact of a droplet with two margins of hydrophobic stripe at the same time, the symmetry condition yields r_{max} as (see Fig. 1a):

$$r_{max,1} = \frac{W_{DWC}}{2\sin\theta} \tag{3}$$

Fig. 1b shows general case for which a droplet center-mass location deviates from the hydrophobic stripe centerline by Δ. The droplet only contacts one margin of the hydrophobic stripe, called one-side-suction OSS in this paper. Correspondingly, r_{max} is

$$r_{max,2} = \frac{x}{\sin\theta} \tag{4}$$

Fig. 1a is a special case of Fig. 1b when $\Delta = 0$ or $x = W_{DWC}/2$.

For a droplet on hydrophobic surface (see Fig. 1c), the droplet radius at the onset of sliding is [8].

$$r_{slide} = \sqrt{\frac{12}{\pi^2} \times \frac{\sin\theta(\cos\theta_r - \cos\theta_a)}{2 - 3\cos\theta + \cos^3\theta} \times \frac{\sigma}{(\rho_l - \rho_v)g}} \tag{5}$$

where σ is the surface tension, ρ_l and ρ_v are densities of liquid and vapor, respectively, g is the gravity acceleration ($g = 9.8$ m/s^2).

At any x, the droplet detaches the surface in one of the three detachment modes shown in Fig. 1. The criterion for droplet detachment is

$$r_{max,3} = \min\left(\frac{x}{\sin\theta}, r_{slide}\right) \tag{6}$$

A critical width of hydrophobic stripe exists when $r_{max,1}$ in Eq. (3) equals to r_{slide} in Eq. (5):

$$W_{DWC,c} = 2r_{slide}\sin\theta \tag{7}$$

Eqs. (6)–(7) guide the whole computation logic shown in Fig. 2. If $W_{DWC} < W_{DWC,c}$, all droplets detach hydrophobic stripes with DSS and OSS modes. All the condensate liquid mass generated on hydrophobic region is transported to hydrophilic stripe (open channel). Alternatively, if $W_{DWC} > W_{DWC,c}$, droplets detach hydrophobic stripes in a mixing mode of OSS and sliding. The whole hydrophobic stripe width is divided into two regions: OSS region close to the margin and a slide region located at the stripe center (see Fig. 2a). Only the condensate liquid mass on OSS region is transported to hydrophilic stripe. The condensate liquid mass on slide region is self-detached under gravity. Thus, the *full-liquid-mass-transfer* from hydrophobic stripe to hydrophilic stripe is defined for $W_{DWC} < W_{DWC,c}$. Alternatively, the *partial-liquid-mass-transfer* from hydrophobic stripe to hydrophilic stripe is defined for $W_{DWC} > W_{DWC,c}$. The computation is divided into two branches in terms of *full-liquid-mass-transfer* and *partial-liquid-mass-transfer*. Because r_{max} depends on x, the half hydrophobic stripe width is segmented into n grids due to geometry symmetry. Each grid has the size of $\Delta x = W_{DWC}/2n$, and the droplet center-mass location is $x = iW_{DWC}/2n$, where i is the index from the margin location to the hydrophobic stripe centerline. The determination of h_{BI} in Eq. (1) is an integration effect over the whole x locations. Fig. 2b shows the computation strategy. To ensure the computation accuracy, Δx is set as 1 μm. A code to solve the problem is developed on the Matlab platform.

2.2.3. Dropwise condensation on hydrophobic stripe

For dropwise condensation, the heat flux is

$$q_{DWC} = \int_{r_{min}}^{r_c} Q(r)n(r)dr + \int_{r_c}^{r_{max}} Q(r)N(r)dr \tag{8}$$

where $Q(r)$ is the heat transfer rate of a single drop at the size of r, r_{min} is the minimum drop nucleation radius, r_c is the half of average spacing between neighboring nucleation sites. All condensate droplets are divided into two groups. The first group has the size range of $r_{min} < r < r_c$ and population density of $n(r)$. The second group has the size range of $r_c < r < r_{max}$ and population density of $N(r)$.

Except the determination of r_{max} in the above section, the calculation of DWC on hydrophobic stripe is similar to that on purely hydrophobic surface. Based on Gibbs free energy analysis, Graham and Griffith [33] obtained

$$r_{min} = \frac{2T_{sat}\sigma}{h_{lv}\rho_l\Delta T} \tag{9}$$

where h_{lv} is the latent heat of evaporation.

On the other hand, r_c is related to droplet nucleation site density N_c as

$$r_c = \sqrt{\frac{1}{4N_c}} \tag{10}$$

In the literature, there are contradictory statements on how to select N_c. Pound et al. [34] thought that N_c can be related to surface wettability. However, the experiment by Zhao and Beysens [35] did not show an obvious connection between N_c and surface wettability. The common cognition is that N_c is influenced by surface roughness. In this paper, a constant N_c is assumed because smooth stripe surface is used. The value of $N_c = 2.5 \times 10^{11}$ m^{-2} yields the corresponding r_c in micron scale [36]. Our previous studies [7,9] confirmed that the simulations with $N_c = 2.5 \times 10^{11}$ m^{-2} excellently matched the measured heat transfer performance. Thus, $N_c = 2.5 \times 10^{11}$ m^{-2} is recommended in this paper. Kim and Kim [37] also used this value in their simulations.

The heat transfer rate of a single drop is

$$Q(r) = \frac{\pi r^2 \sin^2\theta\left(\Delta T - \frac{2T_{sat}\sigma}{h_{lv}r\rho_l}\right)}{\frac{1+\cos\theta}{2h_i} + \frac{\theta\sin\theta}{4\pi}\frac{r}{\lambda_l} + \frac{\delta_p}{\lambda_p}} \tag{11}$$

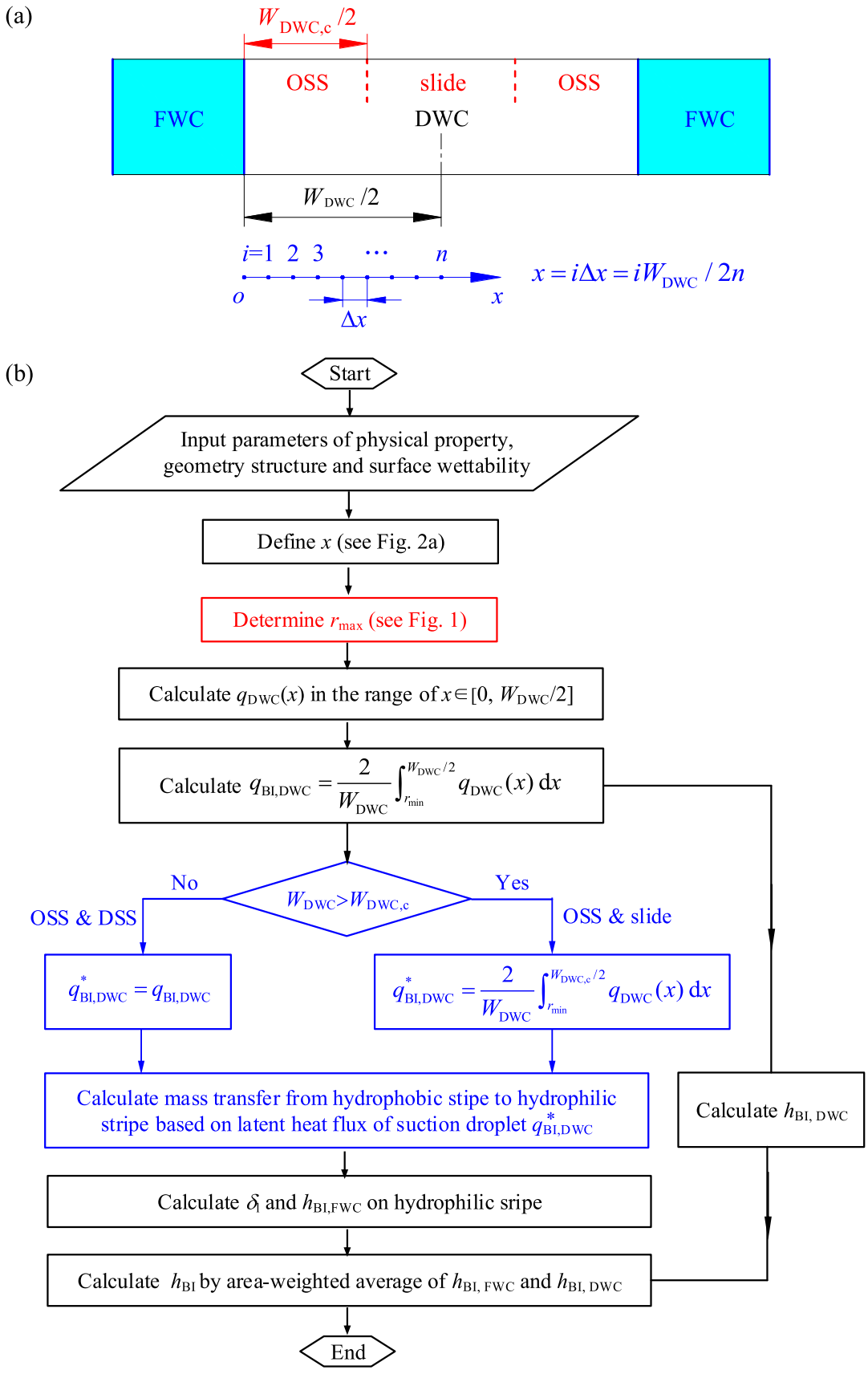

Fig. 2. The computation procedure of condensation heat transfer on biphilic surface.

where λ_l is the thermal conductivity of liquid, which is dependent on T_{sat}, λ_p is the thermal conductivity of coating layer, $\lambda_p = 0.2$ W/(mK) for present application. The determination of heat transfer coefficient at vapor-liquid interface h_i can be found in Ref. [9].

The population density of small droplets in the range of $r_{min}<r<r_c$ is

$$n(r) = \frac{r}{3\pi r_c^3 r_{max}} \times \frac{r_c - r_{min}}{r - r_{min}} \times \frac{A_2 r + A_3}{A_2 r_c + A_3} \times \left(\frac{r_{max}}{r_c}\right)^{\frac{2}{3}} \times \exp(B_1 + B_2) \quad (12)$$

The parameters A_2, A_3, B_1 and B_2 can be found in Refs. [38,39].

Physically, r_c also represents the critical droplet size to initiate the droplet coalescence. Considering coalescence, Fevre and Rose [40] gave the population density of large droplets in the range of $r_c<r<r_{max}$:

$$N(r) = \frac{1}{3\pi r^2 r_{max}} \left(\frac{r_{max}}{r}\right)^{2/3} \quad (13)$$

In Eqs. (12) and (13), r_{max} is the upper limit size, which is suitable not only for locally nucleated and growing droplet at x, but also for droplet transported from elsewhere to x after coalescence. Alwazzan et al. [26] and Ghosh et al. [31] observed that when droplets are close to the margin, the coalescence induced sloshing may trigger liquid suction before droplet size reaches r_{max}. Alwazzan et al. [26] showed that the measured droplet size is only decreased by 3–9% compared with the predicted r_{max} not considering the sloshing effect, concluding the weak sloshing effect on r_{max}. The sloshing effect can only occur when droplets are very close to the margin, which can be regarded as a special case. Thus, the sloshing effect was not considered to determine r_{max}.

DWC on hydrophobic surface can have the sweeping effect to clean droplets in sliding path (see Fig. 3a), which is reflected in Eqs. (12)–(13) by considering a sweeping time in the parameters B_1 and B_2 [38]. Condensation on biphilic surface still has the sweeping effect. For wide hydrophobic stripe, the droplet sliding induced sweeping is similar to Fig. 3a. For narrow hydrophobic stripe, droplets represented by red color between the suction droplet and the margin can be cleaned by the suction droplet (see Fig. 3b), which is observed by Garimella et al. [23] and Alwazzan et al. [26]. The sweeping effect on biphilic surface is still considered in Eqs. (12)–(13).

The above descriptions show that r_{max} influences DWC in three ways: (1) r_{max} determines the upper limit of integral in Eq. (8). (2) r_{max} influences $n(r)$ for small droplets group in Eq. (12). (3) r_{max} influences $N(r)$ for large droplets group in Eq. (13). Because r_{max} depends on x, $n(r)$, $N(r)$ and q_{DWC} are varied versus x, the average heat flux on hydrophobic stripe is

$$q_{BI,DWC} = \begin{cases} \dfrac{2\int_{r_{min}}^{W_{DWC}/2}\int_{r_{min}}^{x} Q(r)n(r)\mathrm{d}r\mathrm{d}x}{W_{DWC}}, & W_{DWC} < 2r_c \\ \dfrac{2\int_{r_{min}}^{r_c}\int_{r_{min}}^{x} Q(r)n(r)\mathrm{d}r\mathrm{d}x + 2\int_{r_c}^{W_{DWC}/2} q_{DWC}(x)\mathrm{d}x}{W_{DWC}}, & W_{DWC} > 2r_c \end{cases} \quad (14)$$

Condensation heat transfer coefficient on hydrophobic stripe is

$$h_{BI,DWC} = \frac{q_{BI,DWC}}{\Delta T} \quad (15)$$

2.2.4. Filmwise condensation on hydrophilic stripe

Biphilic surface is circular with a radius R, which is convenient for comparison with experiments. The number of hydrophobic stripes or hydrophilic stripes is $\bar{n}$:

$$\bar{n} = \frac{2R}{W_{FWC} + W_{DWC}} \quad (16)$$

The areas of hydrophilic stripes and hydrophobic stripes over the circular biscuit are A_{DWC} and A_{FWC}:

$$A_{FWC} = \frac{W_{FWC}}{W_{DWC} + W_{FWC}}\pi R^2, \quad A_{DWC} = \frac{W_{DWC}}{W_{DWC} + W_{FWC}}\pi R^2 \quad (17)$$

Volume flow rate in open channels (hydrophilic stripes) comes from those of self-condensation in open channels V_{FWC} and transferred from hydrophobic stripes V_{trans}:

$$V = V_{FWC} + V_{trans} \quad (18)$$

$$V_{FWC} = \frac{h_{BI,FWC}\Delta T}{\rho_l h_{lv}} A_{FWC}, \quad V_{trans} = \frac{q^*_{BI,DWC}}{\rho_l h_{lv}} A_{DWC} \quad (19)$$

Where $q^*_{BI,DWC}$ is the effective heat flux on hydrophobic stripe for liquid generation to be transferred to hydrophilic region, which is

$$q^*_{BI,DWC} = \begin{cases} q_{BI,DWC}, & W_{DWC} \le W_{DWC,c} \text{ for full-liquid-mass-transfer} \\ \dfrac{2\int_{r_{min}}^{r_{slide}\sin\theta} q_{DWC}(x)\mathrm{d}x}{W_{DWC}}, & W_{DWC} > W_{DWC,c} \text{ for partial-liquid-mass-transfer} \end{cases} \quad (20)$$

The mass conservation in open channels yields

$$V_{FWC} + V_{trans} = \bar{u} \cdot (W_{FWC}\delta_l) \cdot \bar{n} \quad (21)$$

where $\bar{u}$ is the mean liquid film velocity in open channel containing hydrophilic stripe, δ_l is the liquid film thickness. Based on Ref. [41], the following equation exists:

$$\bar{u} = \frac{\rho_l g}{3\mu_l}\delta_l^2 \quad (22)$$

Combining Eqs. (19), (21) and (22) yields

$$\delta_l = \left[\frac{3\pi R\mu_l\left(a \cdot q^*_{BI,DWC} + h_{BI,FWC}\Delta T\right)}{2\rho_l^2 g h_{lv}}\right]^{1/3} \quad (23)$$

where $a = W_{DWC}/W_{FWC}$. The relationship between heat transfer coefficient and thermal resistance writes

$$h_{BI,FWC} = \frac{1}{\frac{1}{h_i} + \frac{\delta_l}{\lambda_l}} \quad (24)$$

Coupling Eqs. (23)–(24) achieves the liquid film thickness δ_l and condensation heat transfer coefficient $h_{BI,FWC}$.

3. Results and discussion

3.1. Comparison with existing models and experimental data

The effect of droplet detachment modes on maximum droplet sizes and heat transfer on hydrophobic /hydrophilic stripes are analyzed, in which the water-vapor condensation was treated with $T_{sat} = 60°C$, $\Delta T = 5$ K, $\theta = 110°$, $\theta_a = 120°$, $\theta_r = 105°$, $\delta_p = 1$ nm and

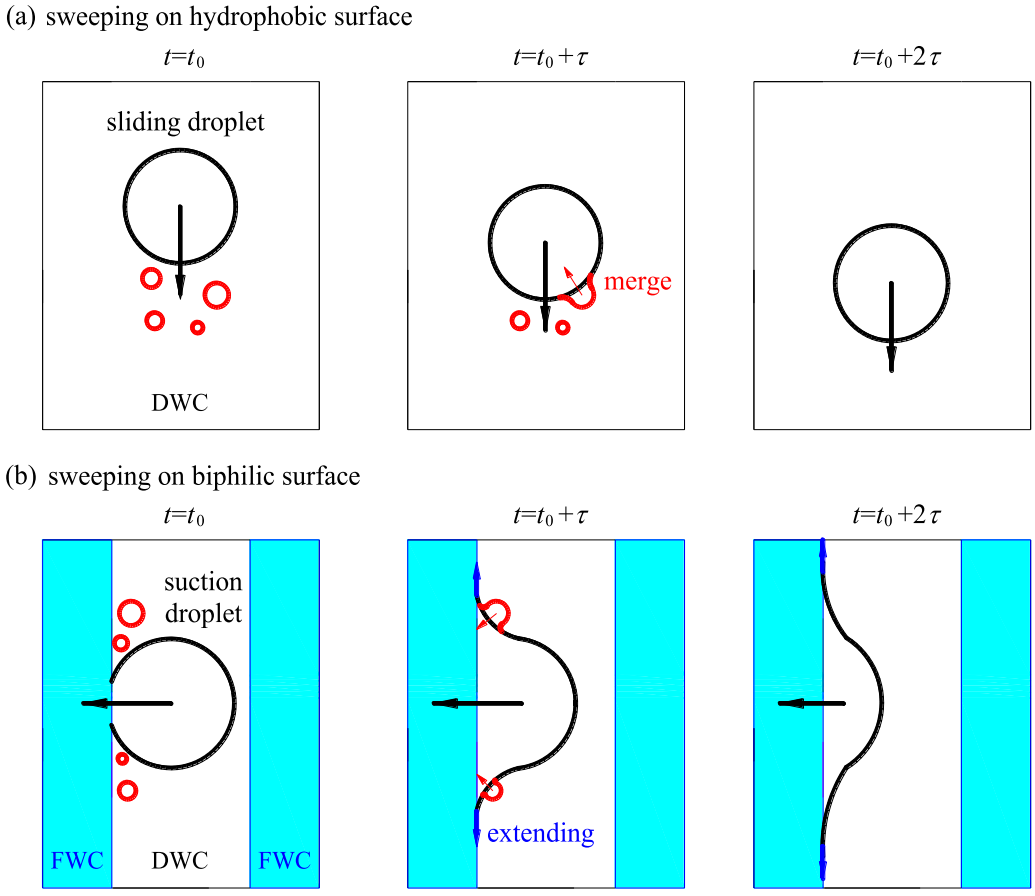

Fig. 3. The droplet sweeping effect (a: on hydrophobic surface, b: on biphilic surface).

$W_{FWC} = 0.2$mm (see Fig. 4). The $r_{max,1}$ criterion for DSS mode behaves a linear relationship of r_{max} versus W_{DWC} with a slope of $1/(2\sin\theta)$. This is a special case for droplet removal and over-estimates r_{max} on hydrophobic stripes. Heat transfer coefficients on hydrophobic stripes $h_{BI,DWC}$ are decreased with the increase of W_{DWC}. The $h_{BI,DWC}$ values are inter-crossed with h_{HB} on purely hydrophobic surface. Beyond the crossing point, the larger the W_{DWC}, the larger deviation of $h_{BI,DWC}$ from h_{HB} is. Physically, condensation heat transfer with sufficiently wide W_{DWC} should approach that on a purely hydrophobic surface. The results predicted by the $r_{max,1}$ criterion is against this variation trend regarding W_{DWC}. Thus, the $r_{max,1}$ criterion should be revised.

A droplet with its center-mass location deviating from a hydrophobic stripe centerline can be sucked by the closer margin to yield the $r_{max,2}$ criterion for OSS mode. The maximum droplet radius r_{max} depends on the droplet center-mass location x. At any x, $r_{max,2}$ for OSS mode is smaller than $r_{max,1}$ for DSS mode. The OSS effect (one-side-suction) obviously reduces droplet size on hydrophobic stripes to enhance condensation heat transfer there.

The $r_{max,3}$ criterion for mixed droplet detachment mode coincides with $r_{max,2}$ criterion for $W_{DWC} \le W_{DWC,c}$, under which droplet sliding does not occur. The mixed droplet detachment modes take place for $W_{DWC} > W_{DWC,c}$, under which droplets on the center region of hydrophobic stripe detach by self-sliding, droplets on the two side regions of hydrophobic stripe are sucked by the corresponding margin (see Fig. 2a). It is noted that $W_{DWC,c}$ is the critical width of hydrophobic stripe for droplet sliding occurring at hydrophilic stripe centerline ($x = W_{DWC}/2$). For a droplet center-mass deviating from the centerline such as $x = W_{DWC}/4$ shown in Fig. 4a, the transition from OSS to sliding takes place at larger W_{DWC} than $W_{DWC,c}$. Once transition from OSS to sliding occurs, r_{slide} is smaller than $r_{max,2}$ and not dependent on W_{DWC}. For wider hydrophobic stripes and with the help of droplet sliding effect, heat transfer coefficients on hydrophobic stripes are larger than those predicted by the $r_{max,1}$ and $r_{max,2}$ criteria. With continuous increase of W_{DWC}, the predicted heat transfer using the $r_{max,3}$ criterion approaches that on purely hydrophobic surface (see Fig. 4b), supporting the physical fact regarding the variation trend of W_{DWC}.

Fig. 4c and d shows the effect of droplet detachment modes of hydrophobic stripe on liquid film thicknesses and heat transfer on hydrophilic stripe (open channel). The DSS mode keeps larger droplet size to weaken condensation on hydrophobic stripe, decreasing mass transfer from hydrophobic stripe to hydrophilic stripe. Thus, the DSS mode decreases liquid film thicknesses in open channel. On the contrary, the OSS mode maintains smaller droplet size on hydrophobic stripe to increase liquid film thicknesses in open channel. The DSS mode overestimates the heat transfer on hydrophilic stripe compared with the OSS mode. Besides, OSS mode under-predicts heat transfer on hydrophilic stripe for $W_{DWC} > W_{DWC,c}$ due to *partial-liquid-mass-transfer* from hydrophobic stripe to hydrophilic stripe induced by droplet self-sliding.

In summary, compared with DSS, the OSS effect maintains smaller droplets on hydrophobic stripes, which is useful to improve heat transfer there. The OSS effect keeps thicker liquid film to weaken heat transfer in open channel. The wider hydrophobic stripe with the sliding effect enhances heat transfer for both hydrophobic part and hydrophilic part.

Few experiments are available for comparison with present predictions. Peng et al. [27] performed condensation experiment

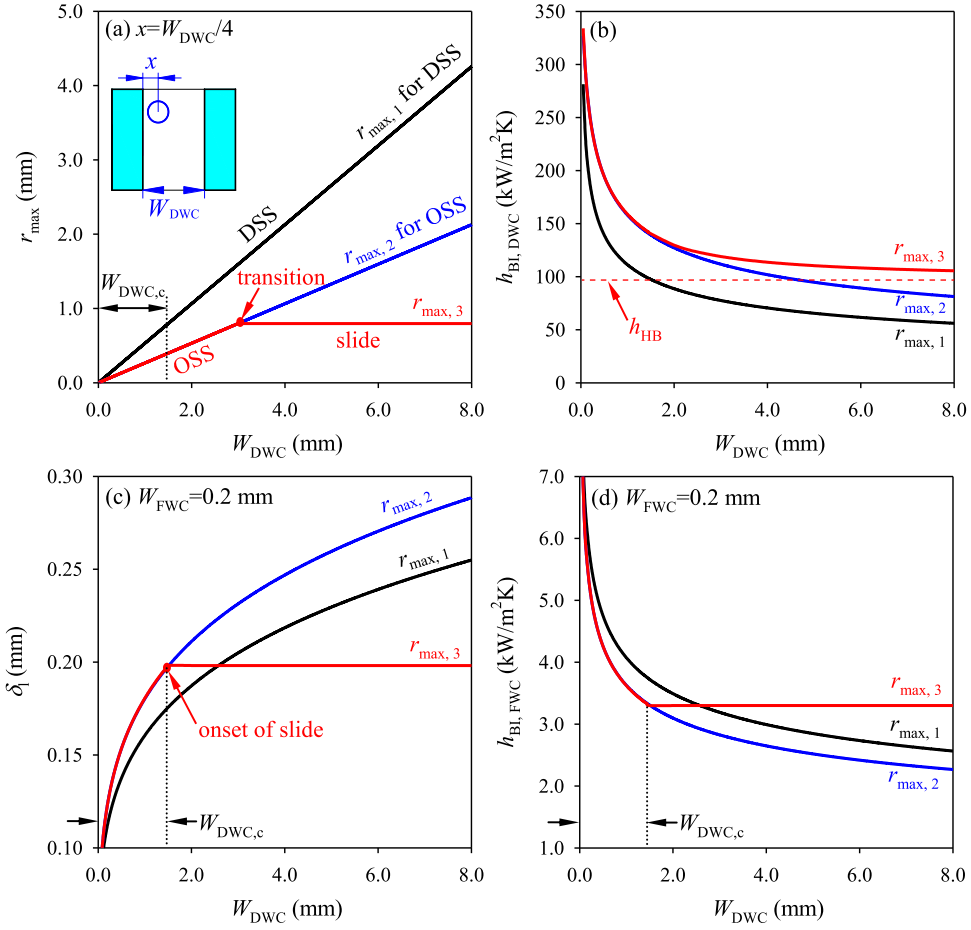

Fig. 4. Effect of droplet detachment modes on maximum droplet size on hydrophobic stripe (a), liquid film thickness in open channel (c) and heat transfer on hydrophobic/hydrophilic stripes (b & d) with $T_{sat}=60$ °C, $\Delta T=5$ °C, $\theta=110°$, $\theta_a=120°$, $\theta_r=105°$, $\delta_p=1$ nm, $W_{FWC}=0.2$ mm.

on vertically biphilic surface, having a circular shape with a diameter of 26.5 mm. The substrate was copper. Each hydrophobic stripe was coated by a thin n-octadecyl mercaptan layer formed by the molecules self-origination mechanism. The wettability parameters are $\theta=120°$, $\theta_a=142°$, $\theta_r=102°$. Each hydrophobic stripe had the width in the range of 0.46–2.30 mm. Each hydrophilic stripe was sandblasted to avoid being coated by n-octadecyl mercaptan monolayer. The hydrophilic stripe width was in the range of 0.44–2.50 mm. The experiment was performed in a pure water-vapor environment at atmospheric pressure. The surface subcooling was in the range of 0.5–11.0 °C. The overall heat flux on biphilic surface was defined as $q_{BI}=h_{BI}\cdot\Delta T$.

The predicted heat fluxes are compared with experiment data by Ref. [27]. Our predictions use the $r_{max,3}$ criterion, and simulations by Peng et al. [28] use the $r_{max,1}$ criterion. Fig. 5a–c shows that the $r_{max,1}$ criterion obviously under-predicts the measured heat flux. Fig. 4 indicates that the $r_{max,1}$ criterion apparently overestimates droplet sizes to under-predict condensation performance on hydrophobic stripes. Even though the $r_{max,1}$ criterion raises condensation heat transfer coefficient in open channel compared with the $r_{max,2}$ criterion for OSS mode, the overall condensation heat flux predicted by the $r_{max,1}$ criterion is quite smaller than the measured values. This is because the condensation heat transfer coefficient on hydrophobic stripes was one to two orders higher than that on hydrophilic stripes.

The condensation model using our newly proposed $r_{max,3}$ criterion excellently matches the measured q_{BI} (see Fig. 5a, b and d). Two reasons explain the good prediction results: (1) The $r_{max,3}$ criterion includes the OSS mode reflects practical condition. Droplets can populate anywhere on hydrophobic stripes. For any droplet center-mass deviating from hydrophobic stripe centerline, the liquid suction does occur once the droplet contacts the closer margin. The DSS mode is a special case for zero deviation. (2) Corresponding to experimental conditions reported in Ref. [27], $W_{DWC,c}=1.85$mm. For wider hydrophobic stripe such as $W_{DWC}=2.30$ mm, the droplet sliding occurs, which is reasonably simulated in our model. Fig. 5c–d gives the errors between model predictions and measured values. The model predictions using the $r_{max,1}$ criterion yield $e_R=-31.50\%$, $e_A=31.54\%$ and $\sigma_n=63.77\%$. On the contrary, the predictions using our newly $r_{max,3}$ criterion gave $e_R=-5.52\%$, $e_A=12.12\%$ and $\sigma_n=12.99\%$. The deviations of e_R, e_A, σ_n are the average deviation, mean absolute deviation and standard deviation, respectively, which are defined in Ref. [42].

3.2. The optimal width of hydrophobic stripe

For biphilic surface, the two kinds of stripes have different functions. Hydrophobic stripes function as the major condensation surface, because dropwise condensation has one to two magnitudes higher heat transfer coefficients than filmwise condensation. Alternatively, hydrophilic stripes function as the liquid transport channel. Previous studies focus on decreasing hydrophobic stripe width W_{DWC} to improve heat transfer [21–24]. Here, the optimal width of hydrophobic stripe W^o_{DWC} is analyzed and the effect parameters are discussed.

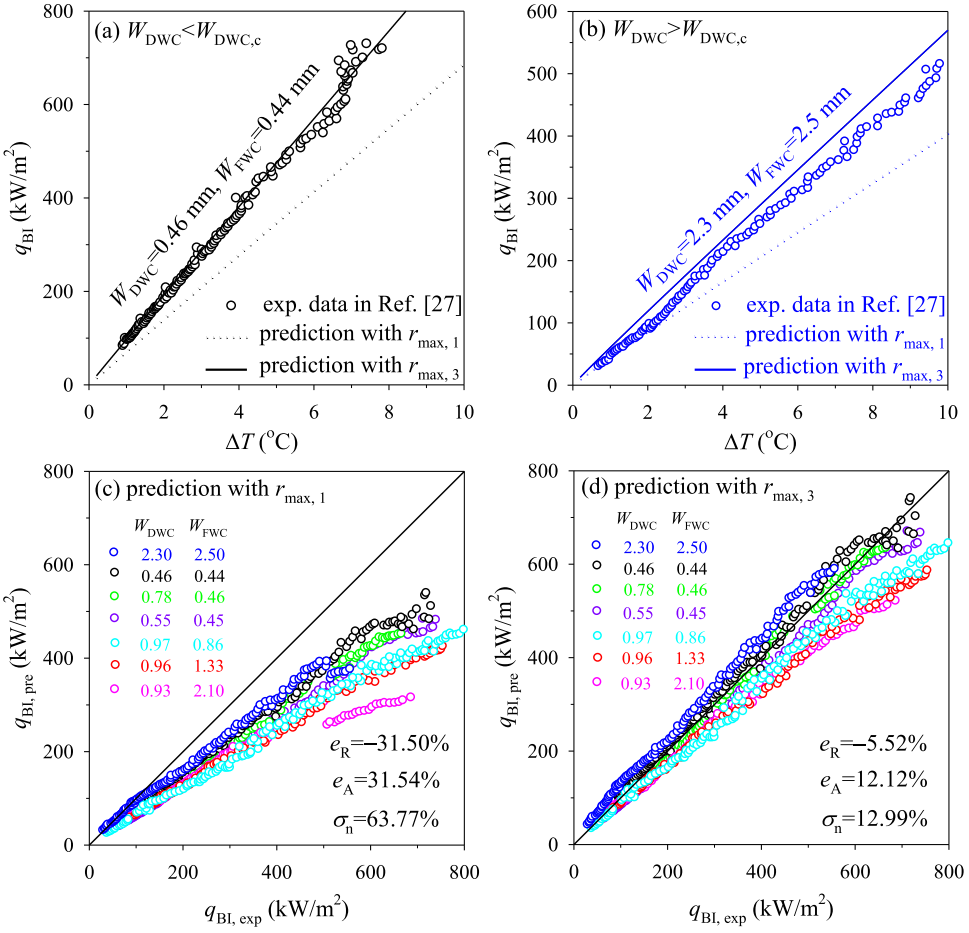

Fig. 5. The comparison of present predictions with experiment data (T_{sat} = 100 °C, θ = 120°, θ_a = 142°, θ_r = 102°, δ_p = 1 nm, N_c = 2.5 × 10^{11}, $W_{DWC,c}$ = 1.85 mm).

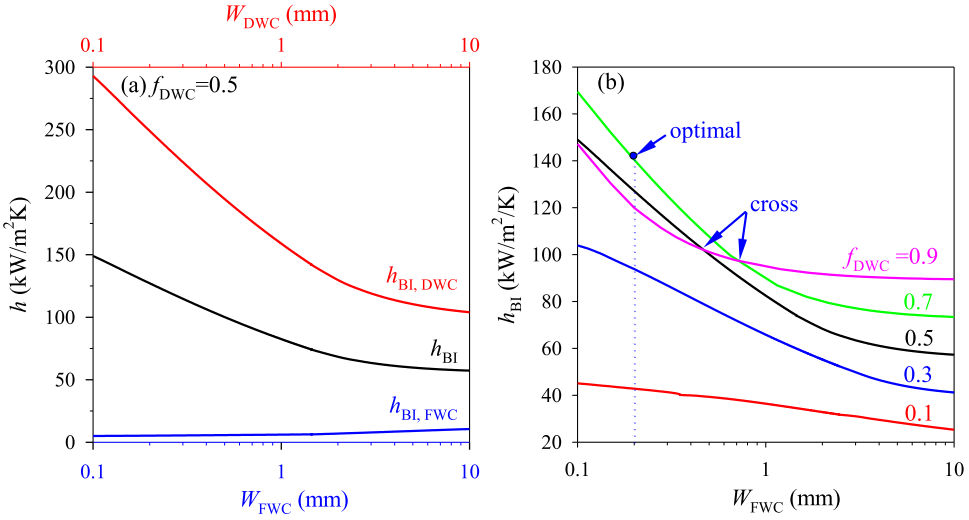

Fig. 6. Effect of f_{DWC} on condensation heat transfer of biphilic surface (T_{sat} = 60 °C, ΔT = 5 °C, θ = 110°, θ_a = 120°, θ_r = 105°, δ_p = 1 nm).

3.2.1. Why does the optimal width of hydrophobic stripe exists?

It is noted that f_{DWC} is the ratio of hydrophobic stripe width relative to the total width of the two regions. Both W_{DWC} and W_{FWC} shall be changed simultaneously at given f_{DWC}. Fig. 6a shows that with increase of $W_{FWC,}$ both $h_{BI,DWC}$ and h_{BI} are decreased, but $h_{BI,FWC}$ are slightly increased, indicating that the heat transfer performance varies monotonously at given f_{DWC}. The h_{BI}~W_{FWC} curves are plotted in Fig. 6b for different f_{DWC}. These curves may intersect. Before the crossing point, an optimal f_{DWC} (or W_{DWC}) exists to generate a maximum h_{BI} for fixed W_{FWC}. Practically, the fabrication process controls W_{DWC} and W_{FWC} directly instead of f_{DWC}. Thus, it is more interesting to search the optimal W_{DWC} when W_{FWC} is fixed.

Fig. 7 plots overall heat transfer coefficients h_{BI} versus W_{DWC} covering the range of 10 μm−10.0 mm at W_{FWC} = 0.2mm. The h_{BI}~W_{DWC} curve indicates an optimal point marked as

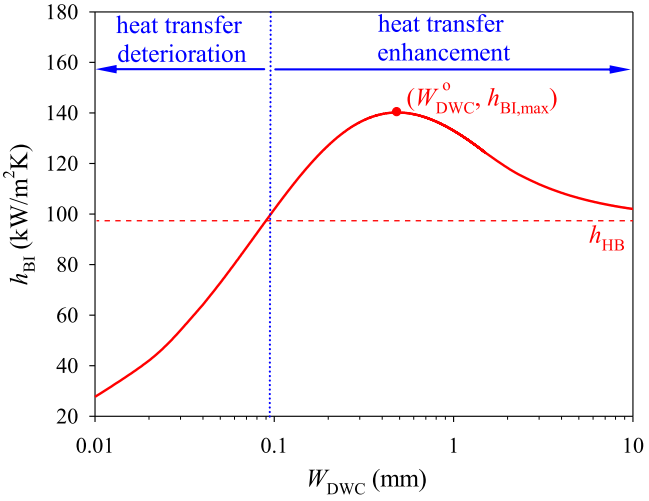

Fig. 7. The overall heat transfer coefficients on biphilic surface h_{BI} dependent on hydrophobic stripe widths W_{DWC} at fixed hydrophilic stripe width W_{FWC} with $T_{sat} = 60$ °C, $\Delta T = 5$ °C, $\theta = 110°$, $\theta_a = 120°$, $\theta_r = 105°$, $\delta_p = 1$ nm and $W_{FWC} = 0.2$ mm.

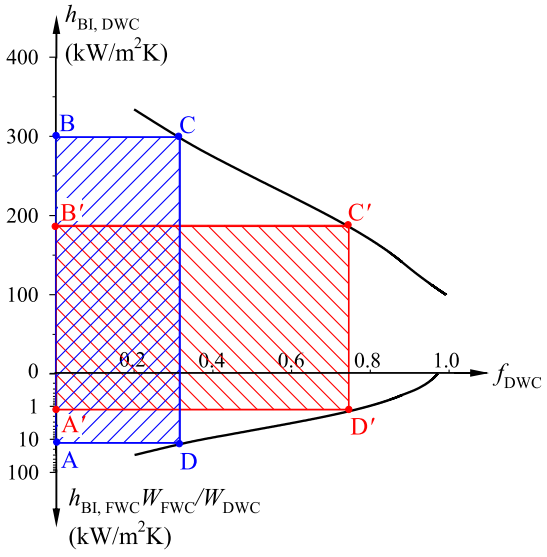

Fig. 8. The shaded rectangular area explaining why an optimal width of hydrophobic stripe exists with an example case of $T_{sat} = 60$ °C, $\Delta T = 5$ °C, $\theta = 110°$, $\theta_a = 120°$, $\theta_r = 105°$, $\delta_p = 1$ nm, $W_{FWC} = 0.2$ mm.

$(W^{o}_{DWC}, h_{BI,max})$. Heat transfer coefficients increase ahead of the optimal point, but decrease beyond the optimal point. For comparison purpose, heat transfer coefficient on hydrophobic surface with uniform wettability h_{HB} is presented as a dashed line. The curve using our $r_{max,3}$ criterion for biphilic surface intercrosses with the dashed line, indicating biphilic surface not always enhancing heat transfer compared with hydrophobic surface. The heat transfer performance of biphilic surface is divided into a heat transfer deterioration regime and a heat transfer enhancement regime. For very narrow stripe such as W_{DWC}<~100 mm, biphilic surface does not enhance heat transfer. The statement "*the narrow the hydrophobic stripe, the better heat transfer performance is*" is not correct.

Eqs. (1) and (2) are recalled to explain why W^{o}_{DWC} exists. Fig. 8 is plotted with f_{DWC} as horizontal coordinate, $h_{BI,DWC}$ and $\frac{W_{FWC}}{W_{DWC}} h_{BI,FWC}$ as two vertical coordinates. Overall heat transfer coefficient h_{BI} can be represented by the rectangular area ABCD, with the rectangular length marked by $AD = BC = f_{DWC}$, and the rectangular width marked by $AB = CD = h_{BI,DWC} + \frac{W_{FWC}}{W_{DWC}} h_{BI,FWC}$. When W_{DWC} is increased, the rectangular area is changed from ABCD to A'B'C'D'. During this process, f_{DWC} is increased, but $h_{BI,DWC} + \frac{W_{FWC}}{W_{DWC}} h_{BI,FWC}$ is decreased (see Fig. 4). Thus, there exists a hydrophobic stripe width W^{o}_{DWC}, which reflects the competition between the area ratio of hydrophobic stripes to total surface and the local condensation on hydrophobic/hydrophilic stripes regarding the size effect.

3.2.2. Effect of various parameters on the optimal width of hydrophobic stripe and heat transfer

Effect of operating parameters: One would like to know if the optimal width of hydrophobic stripe is changed at different operation parameters. The surface subcooling ΔT and saturation vapor temperature T_{sat} are paid attention here. Heat transfer coefficients dependent on ΔT are shown in Fig. 9a at $W_{DWC} = 0.2$ mm. Due to smaller droplets on hydrophobic stripe, heat transfer coefficients $h_{BI,DWC}$ are significantly larger than h_{HB} on hydrophobic surface with uniform wettability. Both $h_{BI,DWC}$ and h_{HB} are almost constant with varied ΔT. Due to the liquid mass transfer from hydrophobic stripe to hydrophilic stripe, heat transfer coefficients $h_{BI,FWC}$ are smaller than h_{HL} on hydrophilic surface. Both $h_{BI,FWC}$ and h_{HL} are weakly decreased with increase of ΔT. The weak effect of ΔT on $h_{BI,DWC}$ and $h_{BI,FWC}$ yields almost coincided overall heat transfer coefficients h_{BI} versus hydrophobic stripe widths at different liquid surface subcooling. When ΔT is changed from 2.5 °C to 12.5 °C,

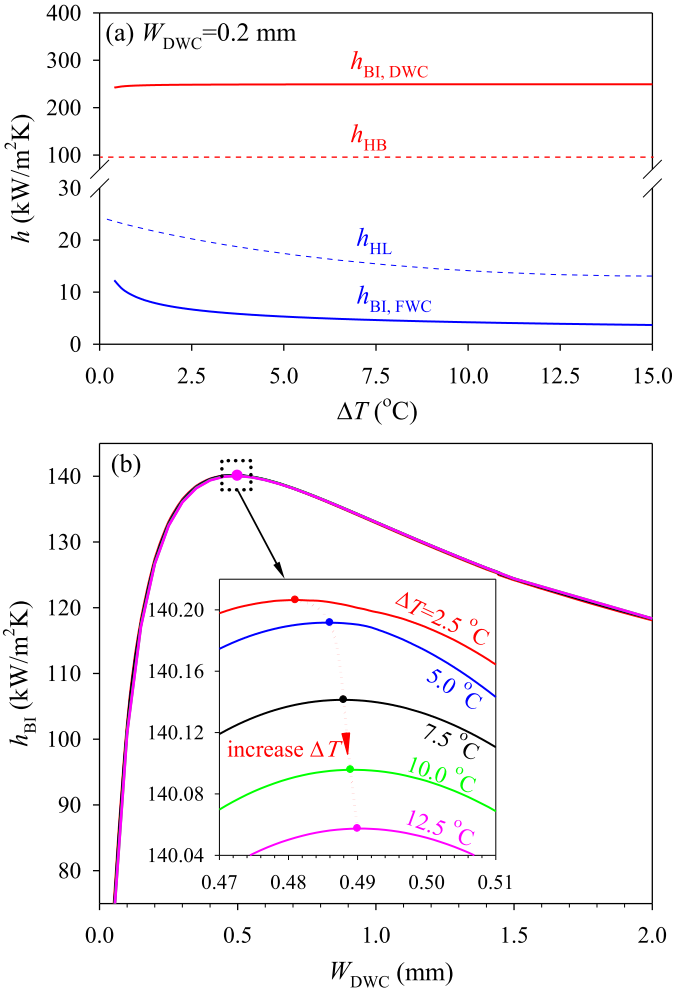

Fig. 9. Effect of surface subcooling on heat transfer coefficients and optimal width of hydrophobic stripe ($T_{sat} = 60$ °C, $\theta = 110°$, $\theta_a = 120°$, $\theta_r = 105°$, $\delta_p = 1$ nm, $W_{FWC} = 0.2$ mm).

Table 2
Physical properties of water-vapor dependent on saturation vapor temperatures

T_{sat} (°C)	P_{sat} (kPa)	ρ_l (kg/m^3)	ρ_v (kg/m^3)	h_{lv} (kJ/kg)	λ_l (mW/mK)	μ_l (mPas)	σ (mN/m)
60	19.95	983.16	0.130	2357.62	654.35	0.466	66.238
90	70.18	965.30	0.424	2282.46	675.25	0.314	60.816
120	198.67	943.11	1.122	2202.09	683.19	0.232	54.968
150	476.16	917.01	2.548	2113.72	682.04	0.182	48.741

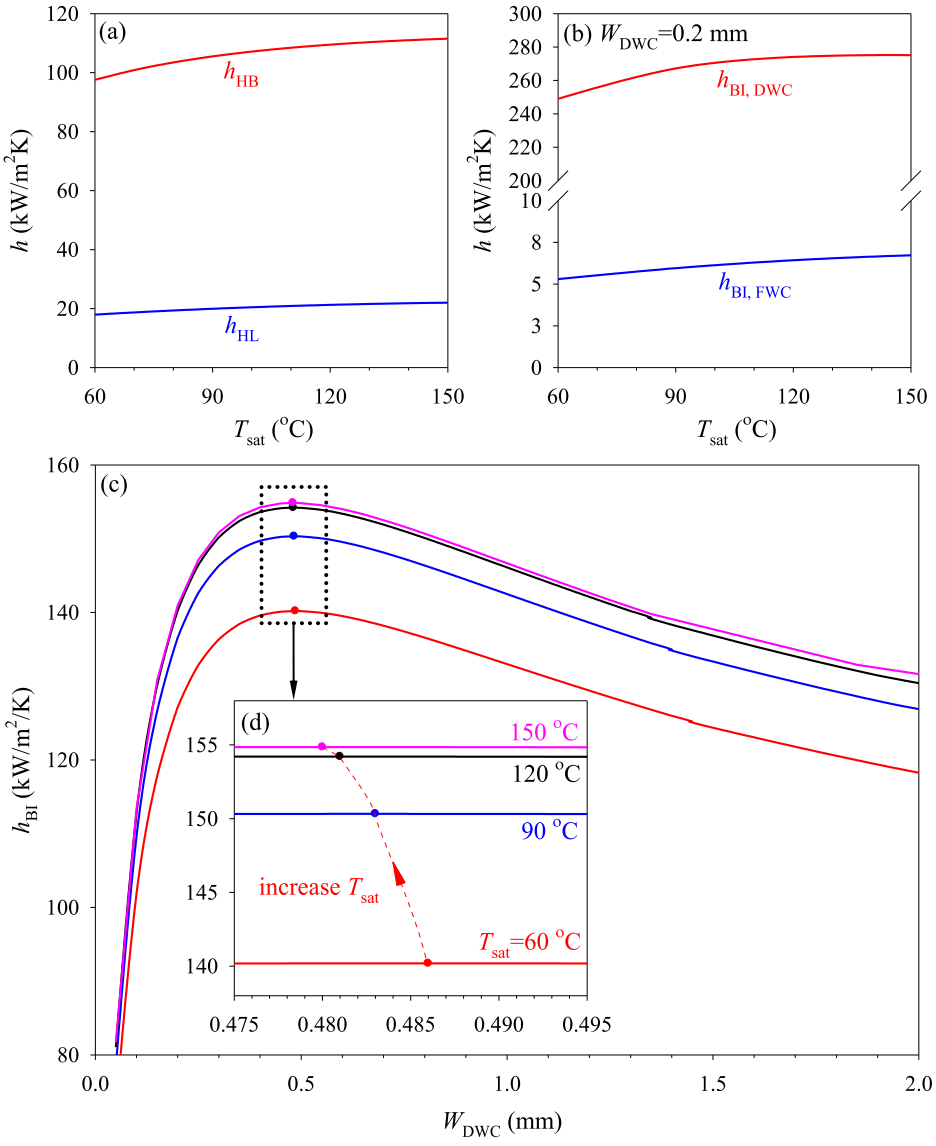

Fig. 10. Effect of saturation vapor temperatures on heat transfer coefficients and optimal width of hydrophobic stripe ($\Delta T = 5$ °C, $\theta = 110°$, $\theta_a = 120°$, $\theta_r = 105°$, $\delta_p = 1$ nm, $W_{FWC} = 0.2$ mm).

$W^o_{DWC}$is changed from 0.481 mm to 0.490 mm. Correspondingly, $h_{BI,max}$ is changed from 140.21 kW/m^{2}K to140.06 kW/m^{2}K (see Fig. 9b).

See Table 2, when saturation temperatures are changed from 60 °C to 150 °C, the increased vapor densities from 0.13 kg/m^3 to 2.548 kg/m^3 improve the interfacial heat transfer coefficients h_i for the enhancement of both dropwise and filmwise condensation. The decreased liquid viscosities decrease liquid film thickness to enhance filmwise condensation. Thus, heat transfer coefficients on hydrophobic surface (h_{HB}), hydrophilic surface (h_{HL}), hydrophobic stripe ($h_{BI,DWC}$) and hydrophilic stripe ($h_{BI,FWC}$) are increased by raising T_{sat} (see Fig. 10a–b). Fig. 10c shows that overall heat transfer coefficients are increased from 140.19 kW/m^{2}K at $T_{sat} = 60$ °C to 154.86 kW/m^{2}K at $T_{sat} = 150$ °C, but the optimal width of hydrophobic stripe is very insensitive to saturation vapor temperatures T_{sat}.

Effect of wettability parameters: Contact angle θ not only influences the single droplet heat transfer, but also affects the droplet density [9]. For single droplet, the increased θ decreases contact area between droplet and condenser surface to weaken heat transfer rate, which is the negative effect. Regarding the effect of θ on droplet density, larger θ ensures smaller drop detachment size r_{max} to enlarge droplet density (see Eqs. (12) and (13)), which is the positive effect. The comprehensive performance depends on the competition of the two effects. The dominance of the positive effect may improve DWC on superhydrophobic nanostructure

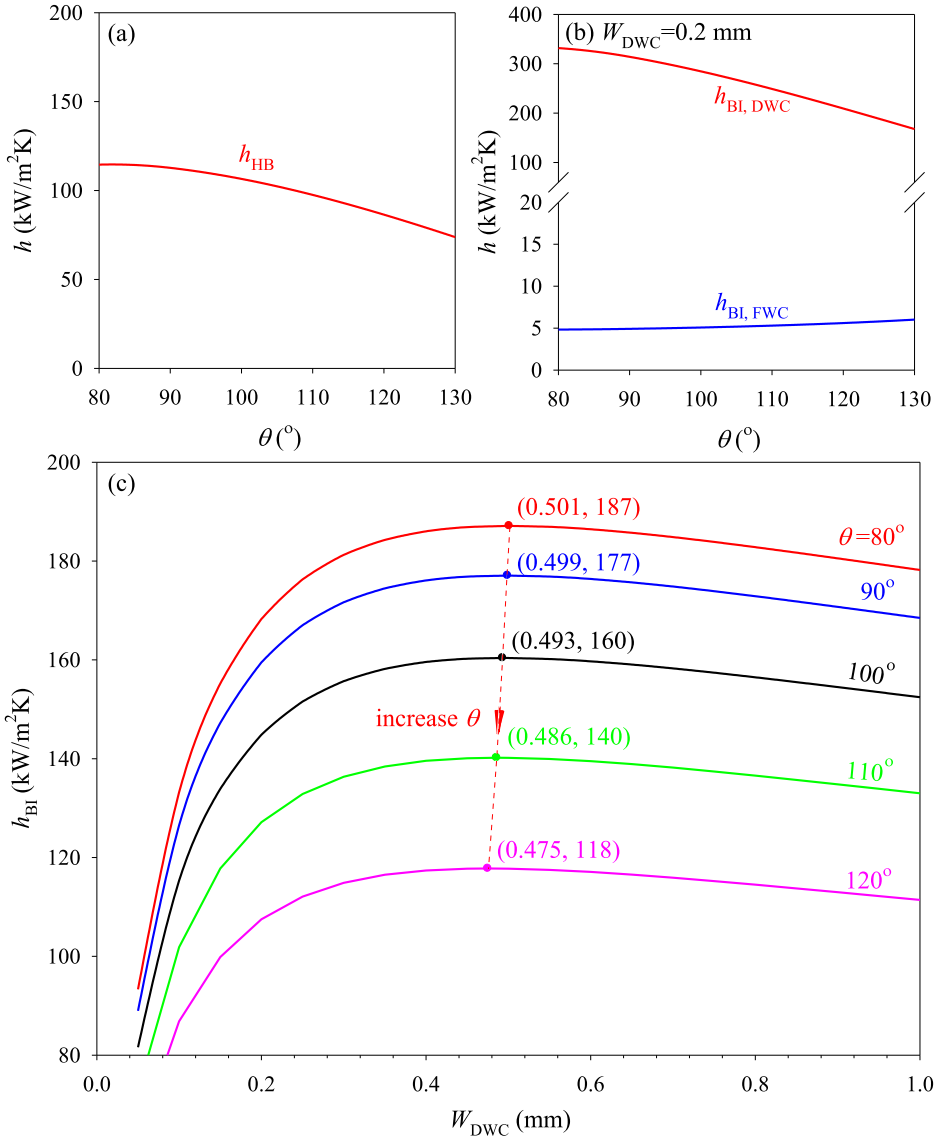

Fig. 11. Effect of equilibrium contact angle on heat transfer coefficients and optimal width of hydrophobic stripe (T_{sat} = 60 °C, ΔT = 5 °C, θ_a = 120°, θ_r = 105°, δ_p = 1 nm, W_{FWC} = 0.2 mm).

surface if θ increases [9]. On the contrary, the dominance of the negative effect can deteriorate DWC on smoothly hydrophobic surface [43]. For smoothly hydrophobic surface, Fig. 11a indicates the decreased heat transfer coefficients when θ increases, agreeing with the predictions in Ref. [43].

For biphilic surface, the increased θ generates two negative effects on DWC. Larger θ not only introduces the difficulty in droplet removal due to raised r_{max} (see Eq. (4)), but also deteriorates droplet heat transfer rate on hydrophobic stripe (see Eq. (11)). Thus, $h_{BI,DWC}$ is decreased with increase of θ. Correspondingly, heat transfer coefficients on hydrophilic stripe $h_{BI, FWC}$ are slightly raised by increasing θ due to the weakened mass transfer from hydrophobic stripe to hydrophilic stripe (see Fig. 11b). The dominant heat transfer on hydrophobic stripe decreases overall heat transfer coefficients when θ is increased. The optimal width of hydrophobic stripe is still insensitive to the variations of θ (see Fig. 11c).

Contact angle hysteresis is $\Omega = \cos\theta_r - = \cos\theta_a$, where θ_r and θ_a are receding contact angle and advancing contact angle, respectively. Ω influences DWC on hydrophobic surface due to varied droplet detachment size in sliding mode. The increased Ω decreases h_{HB} (see Fig. 12a). For biphilic surface with $W_{DWC} < W_{DWC,c}$ such as shown in Fig. 12a, the droplet detachment radius is governed by $r_{max,2}$ in Eq. (4), but has nothing to do with Ω. It is reasonable to observe constant $h_{BI,DWC}$ at varied Ω. The varied Ω has no effect on $h_{BI,FWC}$ on hydrophilic stripe. Overall heat transfer coefficients are plotted versus W_{DWC} covering a wide range from 100 μm to 10 mm in Fig. 12b. Two regimes are observed interfaced at the critical width of hydrophobic stripe $W_{DWC,c}$. All the curves with different Ω coincide with each other ahead of $W_{DWC,c}$. The separated curves are shown at different Ω beyond $W_{DWC,c}$, under which the mixed droplet detachment mode exists including the droplet sliding contribution. Eq. (5) tells us that larger Ω increases r_{slide} to deteriorate heat transfer. Regarding hydrophobic stripe sizes, Ω does not influence the optimal width at all because the optimal width is smaller than the critical width.

Effect of geometrical parameters: Because the increase of coating layer thickness on hydrophobic stripe δ_p raises the substrate thermal resistance underneath a droplet, heat transfer on hydrophobic stripe $h_{BI,DWC}$ is decreased with increase of δ_p. The decrease trend of $h_{BI,DWC}$ is more significant for δ_p >~10 nm. Due to the weakened mass transfer from hydrophobic stripe to hydrophilic stripe, heat transfer coefficients on hydrophilic stripe $h_{BI, FWC}$ are increased

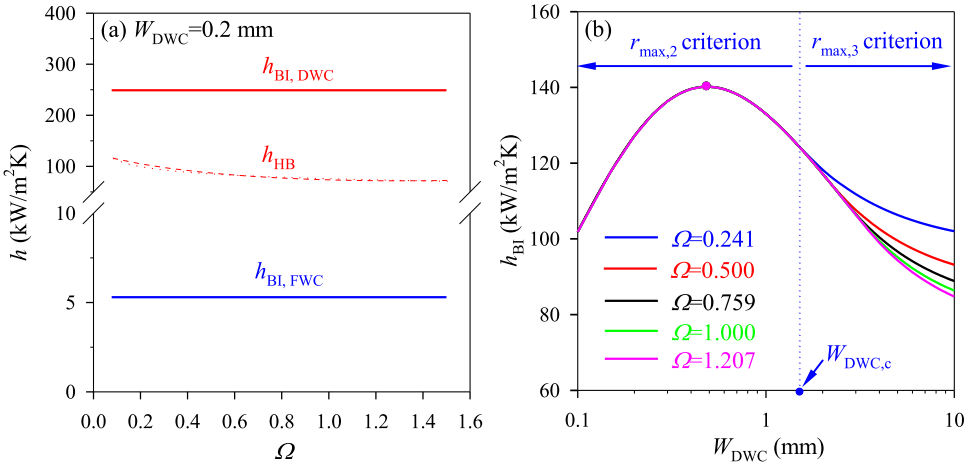

Fig. 12. Effect of contact angle hysteresis on heat transfer coefficients and optimal width of hydrophobic stripe (T_{sat} = 60 °C, ΔT = 5 °C, θ = 110°, δ_p = 1 nm, W_{FWC} = 0.2 mm).

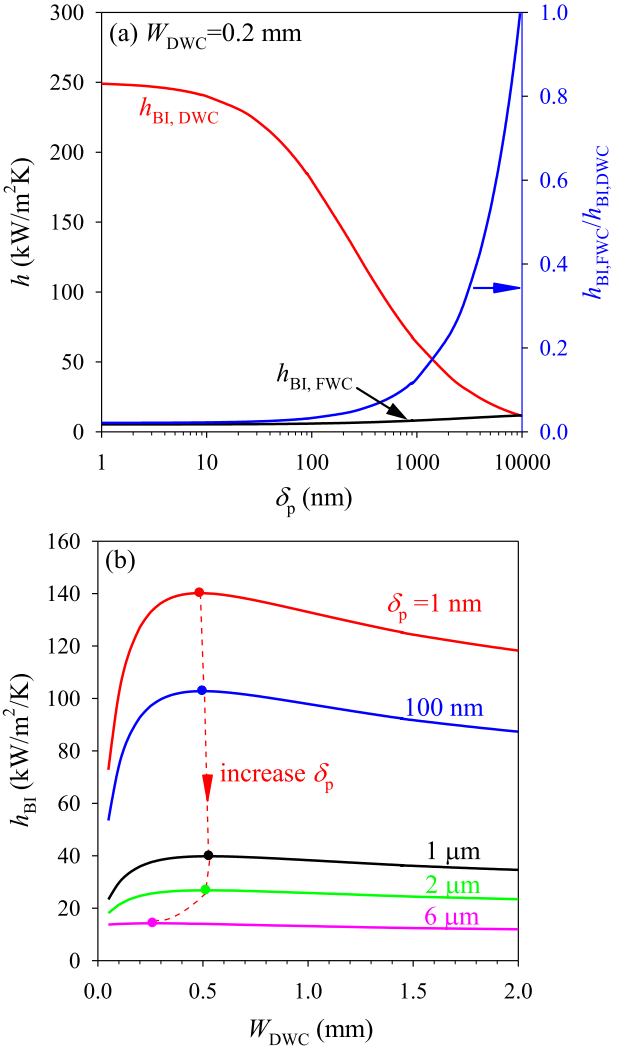

Fig. 13. Effect of hydrophobic coating thickness on heat transfer coefficients and optimal width of hydrophobic stripe (T_{sat} = 60 °C, ΔT = 5 °C, θ = 110°, θ_a = 120°, θ_r = 105°, W_{FWC} = 0.2 mm).

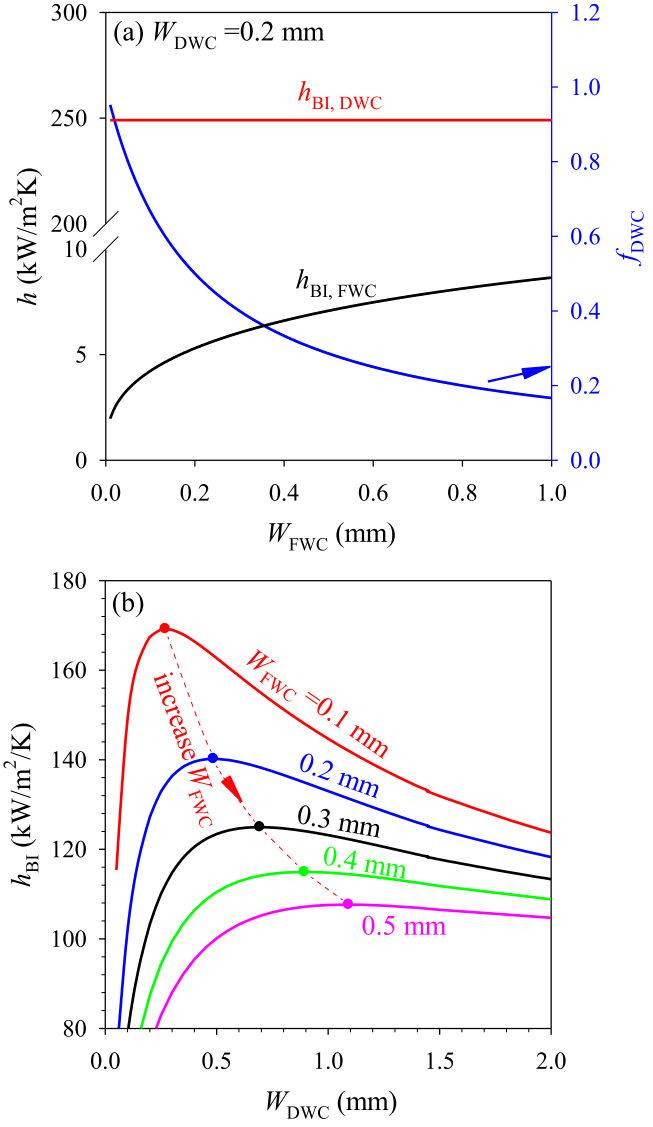

Fig. 14. Effect of hydrophilic stripe widths on heat transfer coefficients and optimal width of hydrophobic stripe (T_{sat} = 60 °C, ΔT = 5 °C, θ = 110°, θ_a = 120°, θ_r = 105°, δ_p = 1 nm).

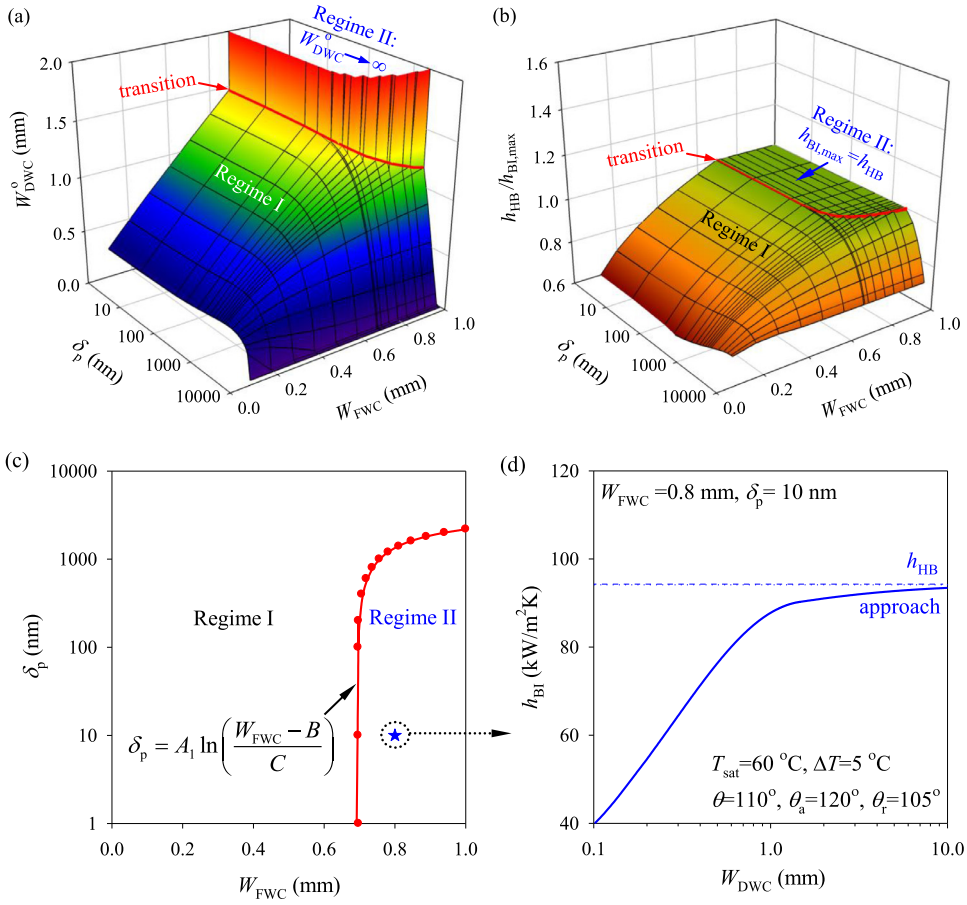

Fig. 15. Optimal conditions and two heat transfer regimes (Regime I for possible heat transfer enhancement and Regime II for heat transfer deterioration, $A_1 = 0.967 \times 10^{-6}$ m, $B = 6.557 \times 10^{-4}$ m, $C = 3.601 \times 10^{-5}$ m).

with increase of δ_p (see Fig. 13a). The above change trends yield obviously deteriorated overall heat transfer on biphilic surface (see Fig. 13b). The ratio of heat transfer coefficient on hydrophilic stripe $h_{BI,FWC}$ to that on hydrophobic stripe $h_{BI,\,DWC}$ is paid attention. With δ_p<~1 mm, hydrophobic stripe dominates heat transfer, but with δ_p>~1 mm, the contribution of hydrophilic stripes is sharply increased. Therefore, with δ_p in the range of 1 nm–1 μm, the optimal width of hydrophobic stripe W^o_{DWC} is insensitive to the variations of δ_p. When δ_p is larger than 1 μm, W^o_{DWC} becomes smaller with increase of δ_p.

Several methods are available to fabricate coating layer on metal substrate. The molecules self-organization technique can make the coating layer thickness in ~1 nm [7,9]. The coating layer thickness can also be ~10 μm using dip-coating method with nanofluid involved [44]. Due to the obvious effect of δ_p on heat transfer, thin coating layer in ~10 nm is recommended for practical applications. The thermal resistance of coating layer (δ_p/λ_p) influences heat transfer rate of a single droplet (see Eq. (11)). In Fig. 13, the coating layer has a thermal conductivity $\lambda_p = 0.200$ W/(mK), which is ~30% of the thermal conductivity of water ($\lambda_l = 0.654$ W/(mK)). The change of λ_p alters $Q(r)$, but it is not necessary to plot h~λ_p curves. This is because such curves display inverse variation trends of h~δ_p curves shown in Fig. 13. In other words, overall heat transfer coefficients are decreased with decrease of λ_p. The coating layer is recommended to have high thermal conductivity for better performance.

Now, how hydrophilic stripe width W_{FWC} influences W^o_{DWC} is analyzed. At given W_{DWC} such as 0.2 mm shown in Fig. 14a, due to one-way mass transfer from hydrophobic stripe to hydrophilic stripe, heat transfer on hydrophobic stripe is not affected by hydrophilic stripe size. For hydrophilic stripe, due to wide spreading of liquid film on stripe width direction, heat transfer is enhanced with increase of its width. One shall remember that f_{DWC} reflects the hydrophobic stripes area contribution to the total heat transfer area. With increase of W_{FWC}, f_{DWC} is decreased to obviously worsen overall heat transfer on biphilic surface. To offset the decreased f_{DWC} factor, the optimal width of hydrophobic stripe should be increased with increase of hydrophilic stripe width, tracking the W_{FWC} variations (see Fig. 14b).

3.3. The possible enhanced heat transfer regime and deteriorated heat transfer regime

Section 3.2 indicates that the optimal width of hydrophobic stripe W^o_{DWC} is hardly influenced by surface subcooling ΔT, vapor saturation temperature T_{sat}, contact angle θ and contact angle hysteresis Ω. The coating layer thickness δ_p and hydrophilic stripe width W_{FWC} do influence W^o_{DWC}. Fig. 15a summarizes the variation trend of W^o_{DWC} with respect to δ_p and W_{FWC}. A red transition curve decouples whole curved surface into two regimes. Below and above the transition curve are Regime I and Regime II, respectively. In Regime I, W^o_{DWC} gets finite value, which linearly increases with increase of W_{FWC} for δ_p<~1 mm, but is affected by both δ_p and W_{FWC} for δ_p>~1 mm. Regime II yields $W^o_{DWC} \to \infty$ corresponding to purely hydrophobic surface. At optimal W^o_{DWC}, the ratios of heat transfer coefficients on purely hydrophobic surface to those on biphilic surface, $h_{HB}/h_{BI,max}$, are plotted versus δ_p and W_{FWC} in Fig. 15b. The value of $h_{HB}/h_{BI,max}$<1 means heat transfer

enhancement using biphilic surface. Regime I demonstrates 67% heat transfer improvement using biphilic surface compared with purely hydrophobic surface, maximally. Regime II achieves the limit heat transfer coefficient of purely hydrophobic surface when $W^{o}_{DWC} \to \infty$.

The red transition curve in Fig. 15a is projected on the $\delta_p - W_{FWC}$ plane in Fig. 15c, which is expressed as

$$\delta_p = A_1 \ln\left(\frac{W_{FWC} - B}{C}\right) \quad (25)$$

where $A_1 = 0.967 \times 10^{-6}$ m, $B = 6.557 \times 10^{-4}$ m, $C = 3.601 \times 10^{-5}$ m, noting that all the units in Eq. (25) are meter. Regime I takes place either at W_{FWC}<~0.7 mm or δ_p>~1 μm. For thicker coating layer such as δ_p>~1 μm, biphilic surface is always populated in Regime I for possible heat transfer enhancement compared with purely hydrophobic surface, no matter what W_{FWC} is. For δ_p<~1 μm, depending on W_{FWC}, the heat transfer can switch from Regime I for possible heat transfer enhancement to Regime II for heat transfer deterioration.

Now, the term *possible heat transfer enhancement* in Regime I is explained. Fig. 15c only plots the relationship between δ_p and W_{FWC} to characterize the transition boundary between the two heat transfer regimes. Heat transfer on biphilic surface is also dependent on W_{DWC}. Fig. 7 is recalled as example case in Regime I. If W_{DWC} approaches W^{o}_{DWC}, heat transfer is definitely enhanced. If W_{DWC} deviates W^{o}_{DWC} too much such as W_{DWC}<~100 μm, heat transfer is deteriorated. Thus, *possible heat transfer enhancement* is named for Regime I.

Regime II occurs with W_{FWC}>~0.7 mmand δ_p<~1 μm. Biphilic surface reaches the up-limit heat transfer coefficient of purely hydrophobic surface when $W^{o}_{DWC} \to \infty$. Corresponding to the star symbol case in Fig. 15c, heat transfer deterioration of biphilic surface with any finite W_{DWC} is observed compared with hydrophobic surface (see Fig. 15d). Thus, *heat transfer deterioration* is named for Regime II.

Finally, to improve condensation heat transfer, strategies are recommended as follows: (1) Hydrophobic coating layer should be as thin as possible such as δ_p<10 nm (see Fig. 13a). (2) Narrow hydrophilic stripe is recommended in ~100 μm scale (see Fig. 14b). (3) Optimal width of hydrophobic stripe is recommend using Fig. 15a. (4) In case thicker hydrophobic coating layer has to be used, biphilic surface is strongly recommended to improve heat transfer (see Fig. 15c).

4. Conclusions

Conclusions are summarized as follows:

- A model was established to deal with condensation on biphilic surface, including sub-models of dropwise condensation on hydrophobic stripe, filmwise condensation on hydrophilic stripe, and a droplet detachment radius r_{max} criterion coupling heat-mass transfer between the two wettabilities regions. Our calculations matched the measured heat transfer data well.
- The r_{max} criterion represents the selection between one-side-suction OSS mode and sliding mode for general consideration. Double-sides-suction DSS mode is a special case of OSS for zero deviation of droplet center-mass from hydrophobic stripe centerline. Critical width of hydrophobic stripe judges the onset of sliding.
- Optimal width of hydrophobic stripe W^{o}_{DWC} is weakly influenced by operating parameters (ΔT, T_{sat}) and wettability parameters (θ, Ω). W^{o}_{DWC} dependent on δ_p and W_{FWC} is summarized in Fig. 15a to guide the biphilic surface design.
- Two heat transfer regimes are interfaced by a $\delta_p - W_{FWC}$ transition boundary. Regime I refers to possible heat transfer enhancement, in which heat transfer is enhanced when W_{DWC} approaches W^{o}_{DWC}, but heat transfer enhancement is not ensured when W_{DWC} deviates W^{o}_{DWC}too much. Regime II refers to heat transfer deterioration, in which heat transfer coefficients are always smaller than those of purely hydrophobic surface.
- Recommendations are proposed to improve condensation heat transfer on biphilic surface.

Declaration of Competing Interest

None

CRediT authorship contribution statement

Jian Xie: Conceptualization, Methodology, Visualization. **Qingting She:** Formal analysis, Writing - original draft. **Jinliang Xu:** Supervision, Project administration, Funding acquisition, Resources. **Cong Liang:** Software, Data curation, Investigation. **Wenxiao Li:** Validation, Writing - review & editing.

Acknowledgements

The authors thank for the funding support by National Natural Science Foundation of China (51806065 and 51436004).

Supplementary materials

Supplementary material associated with this article can be found, in the online version, at doi:10.1016/j.ijheatmasstransfer.2019.119273.

References

[1] W. Nusselt, Die oberflächenkondensation des wasserdampfes, Zeitschrift Des Vereines Deutscher Ingenieure 60 (1916) 541–569.
[2] J. Xie, J.L. Xu, F. Xing, Z.X. Wang, H. Liu, The phase separation concept condensation heat transfer in horizontal tubes for low-grade energy utilization, Energy 69 (2014) 787–800.
[3] J. Xie, J.L. Xu, Y. Cheng, F. Xing, X.T. He, Condensation heat transfer of R245fa in tubes with and without lyophilic porous-membrane-tube insert, Int. J. Heat Mass Transf. 88 (2015) 261–275.
[4] J. Xie, J.L. Xu, C. Liang, Q.T. She, M.J. Li, A comprehensive understanding of enhanced condensation heat transfer using phase separation concept, Energy 172 (2019) 661–674.
[5] H.J. Cho, D.J. Preston, Y.Y. Zhu, E.N. Wang, Nanoengineered materials for liquid-vapour phase-change heat transfer, Nat. Rev. Mater. 2 (2016) 16092.
[6] B.S. Sikarwar, S.K. Muralidhar, Mathematical modelling of dropwise condensation on textured surfaces, Sādhanā 38 (2013) 1135–1171.
[7] J. Xie, J.L. Xu, X. Li, H. Liu, Dropwise condensation on superhydrophobic nanostructure surface, Part I: Long term operation and nanostructure failure, Int. J. Heat Mass Transf. 129 (2019) 86–95.
[8] J. Xie, J.L. Xu, W. Shang, K. Zhang, Mode selection between sliding and rolling for droplet on inclined surface: Effect of surface wettability, Int. J. Heat Mass Transf. 122 (2018) 45–58.
[9] J. Xie, J.L. Xu, W. Shang, K. Zhang, Dropwise condensation on superhydrophobic nanostructure surface, part II: Mathematical model, Int. J. Heat Mass Transf. 127 (2018) 1170–1187.
[10] R.F. Wen, S.S Xu, X.H. Ma, Y.C. Lee, R.G. Yang, Three-dimensional superhydrophobic nanowire networks for enhancing condensation heat transfer, Joule 2 (2018) 269–279.
[11] N. Miljkovic, R. Enright, Y. Nam, K. Lopez, N. Dou, J. Sack, E.N. Wang, Jumping–droplet-enhanced condensation on scalable superhydrophobic nanostructured surfaces, Nano Lett. 13 (2012) 179–187.
[12] J. Zhu, Y.T. Luo, J. Tian, J. Li, X.F. Gao, Clustered ribbed-nanoneedle structured copper surfaces with high-efficiency dropwise condensation heat transfer performance, ACS Appl. Mater. Inter. 7 (2015) 10660–10665.
[13] H.W. Hu, G.H. Tang, D. Niu, Experimental investigation of condensation heat transfer on hybrid wettability finned tube with large amount of noncondensable gas, Int. J. Heat Mass Transf. 85 (2015) 513–523.
[14] E. Olceroglu, M. McCarthy, Self-organization of microscale condensate for delayed flooding of nanostructured superhydrophobic surfaces, ACS Appl. Mater. Inter. 8 (2016) 5729–5736.
[15] D. Torresin, M.K. Tiwari, D.D. Col, D. Poulikakos, Flow condensation on copper-based nanotextured superhydrophobic surfaces, Langmuir 29 (2013) 840–848.

[16] K.R. Murphy, J.B. Boreyko, Enhanced dropwise condensation via droplet removal into opposing wicked evaporator, Proceedings of the 16th International Heat Transfer Conference, IHTC-16 (2018) 10–15.
[17] X.B. Ji, J.L. Xu, H.C. Li, G.H. Huang, Switchable heat transfer mechanisms of nucleation and convection by wettability match of evaporator and condenser for heat pipes: Nanostructured surface effect, Nano Energy 38 (2017) 313–325.
[18] S. Kumagai, S. Tanaka, H. Katsuda, R. Shimada, On the enhancement of filmwise condensation heat transfer by means of the coexistence with dropwise condensation sections, Exp. Heat Transfer 4 (1) (1991) 71–82.
[19] A. Yamauchi, S. Kumagai, T. Takeyama, Condensation heat transfer on various dropwise-filmwise coexisting surface, Heat Transfer-Jap. Res. 15 (1986) 50–64.
[20] S. Kumagai, A. Yamauchi, H. Fukushima, and T. Takeyama, 2nd ASME-JSME Thermal Energy Joint Conference. 4 (1987) 409–415.
[21] M.M. Derby, A. Chatterjee, Y. Peles, M.K. Jensen, Flow condensation heat transfer enhancement in a mini channel with hydrophobic and hydrophilic patterns, Int. J. Heat Mass Transf. 68 (2014) 151–160.
[22] K.S. Yang, K.H. Lin, C.W. Tu, Y.Z. He, C.C. Wang, Experimental investigation of moist air condensation on hydrophilic, hydrophobic, superhydrophilic and hybrid hydrophobic-hydrophilic surfaces, Int. J. Heat Mass Transf. 115 (2017) 1032–1041.
[23] M.M. Garimella, S. Koppu, S.S. Kadlaskar, V. Pillutla, W.Choi Abhijeet, Difference in growth and coalescing patterns of droplets on bi-philic surfaces with varying spatial distribution, J. Colloid Interf. Sci. 505 (2017) 1065–1073.
[24] P.S. Mahapatra, A. Ghosh, R. Ganguly, C.M. Megaridis, Key design and operating parameters for enhancing dropwise condensation through wettability patterning, Int. J. Heat Mass Transf. 92 (2016) 877–883.
[25] J.B. Wu, L.B. Zhang, Y.C. Wang, P. Wang, Efficient and anisotropic fog harvesting on a hybrid and directional surface, Adv. Mater. Interfaces 4 (2) (2017) 1600801.
[26] M. Alwazzan, K. Egab, B.L. Peng, J. Khan, C. Li, Condensation on hybrid-patterned copper tubes (I): Characterization of condensation heat transfer, Int. J. Heat Mass Transf. 112 (2017) 991–1004.
[27] B.L. Peng, X.H. Ma, Z. Lan, W. Xu, R.F. Wen, Experimental investigation on steam condensation heat transfer enhancement with vertically patterned hydrophobic hydrophilic hybrid surfaces, Int. J. Heat Mass Transf. 83 (2015) 27–38.
[28] B.L. Peng, X.H. Ma, Z. Lan, W. Xu, R.F. Wen, Analysis of condensation heat transfer enhancement with dropwise-filmwise hybrid surface: Droplet sizes effect, Int. J. Heat Mass Transf. 77 (2014) 785–794.
[29] T.L. Bergman, A.S. Lavine, F.P. Incropera, D.P. Dewitt, Introduction to Heat Transfer, 6th ed., John Wiley & Sons Inc, Hoboken, 2011.
[30] Y.H. Shang, Y.M. Hou, M. Yu, S.H. Yao, Modeling and optimization of condensation heat transfer at biphilic interface, Int. J. Heat Mass Transf. 122 (2018) 117–127.
[31] A. Ghosh, S. Beaini, B.J. Zhang, R. Ganguly, C.M. Megaridis, Enhancing dropwise condensation through bioinspired wettability patterning, Langmuir 30 (2014) 13103–13115.
[32] K.X. Meng, W.L. Fan, H. Wang, Dynamic scenario simulation of dropwise condensation on a superhydrophobic surface with droplet jumping, Appl. Therm. Eng. 148 (2019) 316–323.
[33] C. Graham, G.P. Griffith, Drop size distributions and heat transfer in dropwise condensation, Int. J. Heat Mass Transf. 16 (2) (1973) 337–346.
[34] G.M. Pound, M.T. Simnad, L. Yang, Heterogeneous nucleation of crystals from vapor, J. Chem. Phys. 22 (1954) 1215.
[35] H. Zhao, D. Beysens, From droplet Growth to film growth on a heterogeneous surface: condensation associated with a wettability gradient, Langmuir 11 (1995) 627–634.
[36] S. Khandekar, K. Muralidhar, Dropwise Condensation on Inclined Textured Surfaces, Springer, New York, 2014.
[37] S. Kim, K.J. Kim, Dropwise condensation modeling suitable for superhydrophobic surfaces, J. Heat Trans. T. ASME 133 (2011) 081502.
[38] M. Abu-Orabi, Modeling of heat transfer in dropwise condensation, Int. J. Heat Mass Transf. 41 (1998) 81–87.
[39] S. Vemuri, K.J. Kim, An experimental and theoretical study on the concept of dropwise condensation, Int. J. Heat Mass Transf. 49 (2006) 649–657.
[40] E.J. Le Fevre, J.W. Rose, A theory of heat transfer by dropwise condensation, in: Proceedings of the 3rd International Heat Transfer Conference, 2, 1966, pp. 362–375.
[41] G.A. O'Neill, J.W. Westwater, Dropwise condensation of steam on electroplated silver surfaces, Int. J. Heat Mass Transf. 27 (9) (1984) 1539–1549.
[42] F. Xing, J.L. Xu, J. Xie, H. Liu, Z.X. Wang, X.L. Ma, Froude number dominates condensation heat transfer of R245fa in tubes: Effect of inclination angles, Int. J. Multiphase Flow 71 (2015) 98–115.
[43] X.L. Liu, P. Cheng, Dropwise condensation theory revisited Part II. Droplet nucleation density and condensation heat flux, Int. J. Heat Mass Transf 83 (2015) 842–849.
[44] J.D. Yuan, Y.B. Wang, J.L. Xu, X.B. Ji, J. Xie, Convective dropwise condensation heat transfer in mini-channels with biphilic surface, Int. J. Heat Mass Transf. 134 (2019) 69–84.